Nonlinear Analysis: Real World Applications 13 (2012) 2079–2095

Contents lists available at SciVerse ScienceDirect

Nonlinear Analysis: Real World Applications

journal homepage: www.elsevier.com/locate/nonrwa

Vortices and vortex sources of multiple vortex interaction systems

Man Jia [a,*], Yuan Gao [b], Fei Huang [c], Sen-yue Lou [a,d,e], Ji-lin Sun [c], Xiao-yan Tang [d]

[a] Department of Physics, Ningbo University, Ningbo 315211, China

[b] School of Agricultural Economics and Rural Development, Renmin University of China, Beijing 100872, China

[c] Physical Oceanography Laboratory and Ocean–Atmosphere Interaction and Climate Laboratory, Ocean University of China, Qingdao 266100, China

[d] Department of Physics, Shanghai Jiao Tong University, Shanghai 200240, China

[e] School of Mathematics, Fudan University, Shanghai 200433, China

ARTICLE INFO

Article history:
Received 15 April 2011
Accepted 9 January 2012

Keywords:
Multiple vortex interaction model
Symmetries and conservation laws
Numerical simulations

ABSTRACT

In this paper, a multiple vortex interaction model (MVIM) is proposed to describe the possible stream–vorticity interaction (SVI) and the vorticity–vorticity interaction (VVI) among vortices. The symmetries and conservation laws of the MVIM show that the SVI preserves the momenta, the vortex momenta and the energies of every vortex, and the interaction energies of every two vortices. However, the VVI destroys the energy conservation property for every vortex. Some special types of exact vortices and vortex source solutions including multiple point vortices, vortex dipoles, vortex multi-poles, fractal cyclons, fractal cyclon dipoles and Bessel vortices (BV) are presented. A special theoretical solution, the first BV is just the usual modon solution which can be used to describe the so-called atmospheric blocking. The second BV is supported by an atmospheric observation, saddle field, occurred over the North Pacific on 26 March, 2009. The characteristic features of vortex interactions are discussed under the MVIM without the β-effect via numerical simulations. Several interaction patterns such as merging, separation, mutual orbiting and absorption are reported. Those interaction behaviors are well consistent with some known fluid mechanical experiments and meteorologic observations.

1. Introduction

Vortices are widely existent phenomena in the physical world. The exploration on vortices has a long history reaching back to the seminal works of Helmholtz and Lord Kelvin [1]. Nowadays, vortices are still arousing consistent interests from physicists, and appear in various attractive fields of physics, such as Bose–Einstein condensates (BECs) [2], nonlinear optics [3], fluid physics [4], plasma science [5], condensed matter physics [6], astrophysics [7], etc. Furthermore, vortex dynamics is not only a rapidly evolving part of physics but also an important subtopic in a wide range of natural scientific fields, such as the biological sciences, earth science, chemistry, mechanics, and so on [8–25].

Vortex interaction is an exciting topic. The pioneering experimental study on vortex interactions was accomplished by Fujiwhara in 1921 [26]. For the binary vortex system in a water tank, Fujiwhara noted that if two vortices were equal in size and strength and spun in the same direction, they would orbit around each other. This type of vortex interactions was called the Fujiwhara effect afterward. Meteorologic observations confirm that the Fujiwhara effect also exists among cyclonic vortices. Particularly, the topic of vortex interaction in two-dimensional flow has been investigated intensively

* Corresponding author. Tel.: +86 574 87609981.
E-mail address: manjia@live.cn (M. Jia).

1468-1218/$ – see front matter © 2012 Elsevier Ltd. All rights reserved.
doi:10.1016/j.nonrwa.2012.01.004

during the last couple of decades. These investigations have included experimental, numerical as well as analytical studies and are reported in numerous papers [27–37].

Especially, in an atmospheric or oceanic system, there exist various kinds of vortices such as tropical cyclones including hurricanes or typhoons [21–24], atmospheric blockings [25], tornadoes [38], subtropical highs [39], polar vortices [40,41] and so on. It is reported that on average, binary cyclone interaction occurs 1.5 times per year over the western North Pacific and 0.33 times per year over the Atlantic [42]. Furthermore, the knowledge of vortex interactions in such an atmospheric or oceanic system has significant practical meaning. For example, it is difficult to predict the tracks of typhoons or hurricanes when they interact with other tropical cyclones. Thus a better understanding on vortex interactions can help to amend the predictions of the typhoon or hurricane tracks, and to avoid tremendous destructions.

In this paper, we propose some interaction models of multiple vortices for the $(2+1)$-dimensional rotating fluid systems, such as the atmospheric and oceanic systems, which can be described by the nonlinear inviscid dissipative and equivalent barotropic vorticity equation (NIDEBVE) in a β-plane channel [43]

$$\omega = \Delta\psi, \quad \Delta \equiv \partial_{xx} + \partial_{yy}, \tag{1}$$

$$\omega_t + [\psi, \omega] + \beta\psi_x = 0, \tag{2}$$

where the velocity

$$\vec{u} = \{u_1, u_2\}$$

is determined by the stream function ψ through

$$u_1 = -\psi_y, \qquad u_2 = \psi_x,$$

and the Jacobian operator $[A, B]$ is defined as

$$[A, B] \equiv A_x B_y - B_x A_y.$$

When $\beta = 0$, the equation system (1)–(2) reduces to the $(2 + 1)$-dimensional Euler equation (EE) which has received numerous studies and many kinds of exact solutions [44] have been presented.

In Section 2, we establish the multiple vortex interaction model (MVIM) with stream–vorticity interaction (SVI) and vorticity–vorticity interaction (VVI). In Section 3, symmetries of the model are studied by using the standard Lie symmetry approach both for the models with and without VVI. The conservation laws of the models are also studied in Section 3, it is found that the SVI preserves conservation of both the energies of every vortex and the interaction energy of every two vortices. In Section 4, some exact vortex source solutions of the models are obtained simply by checking the weak solution conditions. A special type of analytical vortex solutions, the Bessel vortices, is also given when the VVI must be involved. We should mention that in our paper [45] we have obtained the same results. Here we just review it for the concreteness and completeness. After exploring the analytical properties of the MVIM, we turn to the numerical approach in Section 5 for further understanding of the MVIM. The characteristic features of vortex interactions are discussed under the MVIM without the β-effect via numerical simulations. Several interaction patterns such as merging, separation, mutual orbiting and absorption are reported and compared with some known fluid mechanical experiments and meteorologic observations. The last section is a short summary and discussion.

2. A multiple vortex interaction model

In principle, to study the interactions among multiple vortices, one has to obtain an exact multi-vortex solution of Eqs. (1)–(2). However, it is very difficult to find exact analytical multiple vortex solutions for the NINEBVE. In fact, even for the ideal EE case, to find exact analytical multiple vortex solutions is still not easy. Here we try to study the multiple vortices in an alternative way by supposing the following conditions.

(1) Vortex locality. Every vortex is localized for the vorticity ω_i, while the velocities ψ_{ix} and ψ_{iy} may not be localized. That is

$$\omega_i|_{\sqrt{x^2+y^2}\to\infty} = 0, \qquad \{\psi_{iy}, \psi_{ix}\}|_{\sqrt{x^2+y^2}\to\infty} \neq \{0\}. \tag{3}$$

(2) Short range interaction. When two vortices are far away each other, their interactions can be neglected. In other words, every vortex is an approximate solution of the NINEBVE when others are far away from it.

(3) One–one interaction. The interactions for n-vortices can be approximately divided into the summations of 2-vortex interactions.

(4) Total system. The whole system, i.e., the system with the total vorticity and stream function

$$\omega = \sum_{i=1}^{N} \omega_i, \qquad \psi = \sum_{i=1}^{N} \psi_i, \tag{4}$$

is an exact solution of the NINEBVE.

According to the above four assumptions, substituting (4) into NINEBVE (1)–(2), one can obtain the following multiple vortex interaction models (MVIMs)

$$\omega_i = \psi_{ixx} + \psi_{iyy}, \tag{5}$$

$$\omega_{it} + \sum_{j=1}^{N}[\psi_i, \omega_j] - C\sum_{j=1}^{N}[\omega_i, \omega_j] + \beta\psi_{ix} = 0, \tag{6}$$

where $[\psi_i, \omega_j],\ j \neq i$ denotes the i–jth stream–vorticity interactions (SVI) and $[\omega_i, \omega_j]$ denotes the i–jth vorticity–vorticity interactions (VVI). It is clear that when we consider the problem near the i-th vortex, the SVI and VVI terms are small if the other vortices are far away from the i-th vortex because of the localization property of ω_j. In addition, the summation of Eqs. (5) and (6) for i from 1 to N recovers the total system (1)–(2). It should be mentioned that other types of interactions, such as the stream–stream interaction (SSI) like $[\psi_i, \psi_j]$ and the higher order VVI (HOVVI) like $[\omega_i^k, \omega_j^k],\ k > 1$, can be introduced into the model (6). However, the SSI will destroy the assumption (2) due to the nonlocal assumption (1) of the velocity field, while the HOVVI is omitted because of its complexity (related to $2k$-body interaction) and it is smaller than the order of VVI on account of assumption (3), the locality of the vorticity.

It should be mentioned that because (4) solve the NINEBVE, the *arbitrary* function C cannot be determined only by equation system (1)–(2) itself. Actually, one may change the VVI term, $-C\sum_{j=1}^{N}[\omega_i, \omega_j]$, of (6) as $C_i(x, y, t)$ which can be considered as the equivalent force of the other vortices to the i-th vortex except for the SVI under the condition

$$\sum_{i=1}^{N} C_i(x, y, t) = 0.$$

For simplicity, we only take $C_i(x, y, t)$ has the VVI form with constant C. We will point out later that some types of exact solutions of the model do exist for nonzero C.

3. Symmetries and conservation laws

A symmetry of the system (5)–(6),

$$\sigma = \{\sigma_i^{\psi}, \sigma_j^{\omega},\ i, j = 1, 2, \ldots, N\}$$

is a solution of its linearized equation,

$$\sigma_i^{\omega} = \sigma_{ixx}^{\psi} + \sigma_{iyy}^{\psi}, \tag{7}$$

$$\sigma_{it}^{\omega} + \sum_{j=1}^{N}\left\{[\psi_i, \sigma_j^{\omega}] + [\sigma_i^{\psi}, \omega_j]\right\} - C\sum_{j=1}^{N}\left\{[\sigma_i^{\omega}, \omega_j] + [\omega_i, \sigma_j^{\omega}]\right\} + \beta\sigma_{ix}^{\psi} = 0, \tag{8}$$

that means (5)–(6) is form invariant under the transformation

$$\{\psi_i, \omega_i\} \to \{\psi_i, \omega_i\} + \epsilon\{\sigma_i^{\psi}, \sigma_i^{\omega}\}$$

with an infinitesimal parameter ϵ.

For the Lie point symmetries, we have

$$\sigma_i^{\omega} = X\omega_{ix} + Y\omega_{iy} + T\omega_{it} - \Omega_i, \tag{9}$$

$$\sigma_i^{\psi} = X\psi_{ix} + Y\psi_{iy} + T\psi_{it} - \Psi_i, \tag{10}$$

where X, Y, T, Ω_i and Ψ_i are functions of x, y, z, t, ψ_i and ω_i.

Substituting (9)–(10) into (7)–(8) and eliminating ω_i and ψ_{iyy} via (5)–(6) yield the determining equations of X, Y, T, Ω_i and Ψ_i which possess the solutions

$$X = cx + x_0, \qquad Y = cy + y_0, \qquad T = -ct - t_0,$$

$$\sigma_i^{\psi} = 3c\psi_i + \psi_{i0}(t) + \sum_{k=1}^{N} c_{ik}\psi_k,$$

$$\sigma_i^{\omega} = 3c\omega_i + \sum_{k=1}^{N} c_{ik}\omega_k, \tag{11}$$

where x_0, y_0, t_0, c and $c_{ik},\ i, k = 1, 2, \ldots, N$ are constants with the conditions

$$\sum_{i=1}^{N} c_{ik} = 0, \tag{12}$$

$$cC = 0 \tag{13}$$

and $\psi_{i0}(t)$ are arbitrary functions of t.

The equivalent vector form of the symmetries can be written as

$$V = (cx + x_0)\partial_x + (cy + y_0)\partial_y - (ct + t_0)\partial_t + \sum_{i=1}^{N}\left(3c\psi_i + \psi_{i0}(t) + \sum_{k=1}^{N} c_{ik}\psi_k\right)\partial_{\psi_i} + \sum_{i=1}^{N}\left(3c\omega_i + \sum_{k=1}^{N} c_{ik}\omega_k\right)\partial_{\omega_i}. \tag{14}$$

Eq. (14) shows us that the MVIM without VVI is space–time translation invariant (x_0, y_0 and t_0 parts), scaling invariant (c part), time dependent vortex translation ($\psi_{i0}(t)$ parts) and singular ($\det c_{ij} = 0$) rotations of the fields ψ_i and ω_i (c_{ij} parts). For nonzero C, the scaling symmetry is destroyed because of the condition (13).

Now, we are interested in that for the MVIM (5)–(6), what kinds of physical quantities are conserved? Especially, what kind of quantity will be exchanged among different interacting vortices?

A conservation law (CL) means the existence of the conserved density ρ and flows J_1 and J_2 satisfying

$$\rho_t + J_{1x} + J_{2y} = 0. \tag{15}$$

Obviously, all the quantities expressed by the differentiations of x and/or y are conserved due to $(A_x)_t = (A_t)_x$. Therefore, the momenta (with the densities $-\psi_{iy}$ and ψ_{ix}) and the vorticity momenta (with the density $\omega_i = \psi_{ixx} + \psi_{iyy}$) for every vortex are conserved, because they are really total differentiations of some quantities with respect to x or y.

For the vanishing VVI case, the important nontrivial conserved quantities are the energies for every vortex and interaction energies for every two vortices.

Theorem 1 (*Energy Conservation Theorem*)**.** *The MVIM without VVI possesses the conserved energy densities*

$$E_i \equiv \frac{1}{2}(u_{i1}^2 + u_{i2}^2) \equiv \frac{1}{2}(\psi_{iy}^2 + \psi_{ix}^2) \tag{16}$$

for every vortex and the interaction energy density

$$E_{ij} \equiv \psi_{ix}\psi_{jx} + \psi_{iy}\psi_{jy} \tag{17}$$

for every two vortices.

Proof.

$$\begin{aligned}
E_{it} &= \psi_{iy}\psi_{iyt} + \psi_{ix}\psi_{ixt}\\
&= (\psi_i\psi_{iyt})_y - \psi_i\psi_{iyyt} + (\psi_i\psi_{ixt})_x - \psi_i\psi_{ixxt}\\
&= (\psi_i\psi_{iyt})_y + (\psi_i\psi_{ixt})_x - \psi_i\omega_{it}\\
&= (\psi_i\psi_{iyt})_y + (\psi_i\psi_{ixt})_x + \psi_i\{[\psi_i, \omega] - C[\omega_i, \omega] + \beta\psi_{ix}\}\\
&= (\psi_i\psi_{iyt})_y + (\psi_i\psi_{ixt})_x + \frac{1}{2}\left(\psi_i^2\omega_y\right)_x - \frac{1}{2}\left(\psi_i^2\omega_x\right)_y - C\psi_i[\omega_i, \omega] + \frac{1}{2}\beta(\psi_i^2)_x\\
&= \frac{1}{2}(2\psi_i\psi_{iyt} - \psi_i^2\omega_x)_y + \frac{1}{2}(2\psi_i\psi_{ixt} + \psi_i^2\omega_y + \beta\psi_i^2)_x - C\psi_i[\omega_i, \omega].
\end{aligned} \tag{18}$$

From the last step it is clear that E_i is a conserved density if and only if $C = 0$ and the corresponding fluxes possess the forms

$$J_{1i} = -\psi_i\psi_{ixt} - \frac{1}{2}\psi_i^2(\beta + \omega_y), \qquad J_{2i} = \frac{1}{2}\psi_i^2\omega_x - \psi_i\psi_{iyt}. \tag{19}$$

Similarly, for the interaction energy density E_{ij} we have,

$$\begin{aligned}
E_{ijt} &= \psi_{iy}\psi_{jyt} + \psi_{jy}\psi_{iyt} + \psi_{ix}\psi_{jxt} + \psi_{jx}\psi_{ixt}\\
&= (\psi_i\psi_{jyt} + \psi_j\psi_{iyt})_y - \psi_i\psi_{jyyt} - \psi_j\psi_{iyyt} + (\psi_i\psi_{jxt} + \psi_j\psi_{ixt})_x - \psi_i\psi_{jxxt} - \psi_j\psi_{ixxt}\\
&= (\psi_i\psi_{jyt} + \psi_j\psi_{iyt})_y + (\psi_i\psi_{jxt} + \psi_j\psi_{ixt})_x - \psi_i\omega_{jt} - \psi_j\omega_{it}\\
&= (\psi_i\psi_{jyt} + \psi_j\psi_{iyt})_y + (\psi_i\psi_{jxt} + \psi_j\psi_{ixt})_x\\
&\quad + \psi_i\left\{[\psi_j, \omega] - C[\omega_j, \omega] + \beta\psi_{jx}\right\} + \psi_j\{[\psi_i, \omega] - C[\omega_i, \omega] + \beta\psi_{ix}\}\\
&= (\psi_i\psi_{jyt} + \psi_j\psi_{iyt} - \psi_i\psi_j\omega_x)_y + [\psi_i\psi_{jxt} + \psi_j\psi_{ixt} + \psi_i\psi_j(\omega_y + \beta)]_x - C\psi_i[\omega_j, \omega] - C\psi_j[\omega_i, \omega].
\end{aligned} \tag{20}$$

From the last equation, we know that the interaction energy is conserved iff the VVI is neglected while the corresponding fluxes read

$$\begin{aligned}
J_{1ij} &= -\psi_i\psi_{jxt} - \psi_j\psi_{ixt} - \psi_i\psi_j(\beta + \omega_y),\\
J_{2ij} &= -\psi_i\psi_{jyt} - \psi_j\psi_{iyt} + \psi_i\psi_j\omega_x.
\end{aligned}$$

Thus, the theorem is proved. □

Naturally, the conserved densities E_i and E_{ij} imply the conservation of the total energy with the density

$$E_{\text{total}} \equiv \sum_{i=1}^{N} E_i + \sum_{j<i} E_{ij} = \frac{1}{2}\left(\sum_{i=1}^{N} \psi_{ix}\right)^2 + \frac{1}{2}\left(\sum_{i=1}^{N} \psi_{iy}\right)^2. \tag{21}$$

From the theorem we know that for nonzero VVI, $C \neq 0$, there is no additional conserved quantities except for those of the total system. That means the energy exchanges among interacting vortices are introduced by the VVI but not the SVI. In other words, the SVI interaction preserves the energy of the interacting vorticity while the VVI destroys the energy conservation for every single vortex.

4. Exact special vortices and vortex source solutions

To study the concrete exact solutions, we discuss some special examples with and without β term.

4.1. Vortex sources for $\beta = 0$ case

It is not very difficult to verify that the irritating MVIM possess the following exact solutions ($r_i^2 \equiv (x - x_{i0})^2 + (y - y_{i0})^2$, $\theta_i \equiv \arctan\frac{y-y_{i0}}{x-x_{i0}}$)

$$\psi_i = a_i \ln r_i, \quad i = 1, \ldots, k,$$
$$\omega_i = -2a_i\pi\,\omega_{i0}\delta(x_i)\delta(y_i), \tag{22}$$
$$\psi_i = a_i(\ln^2 r_i - \theta_i^2), \quad i = k+1, \ldots, m,$$
$$\omega_i = -4a_i\pi\,\ln(r_i)\delta(x_i)\delta(y_i), \tag{23}$$
$$\psi_i = a_i r_i^{-\delta_i}\sin(\delta_i\theta_i + \theta_{i0}), \quad i = m+1, \ldots, n,$$
$$\omega_i = 2a_i\pi\,\delta_i r^{-\delta_i}\sin(\delta_i\theta_i + \theta_{i0})\delta(x_i)\delta(y_i), \tag{24}$$

and

$$\psi_i = a_i e^{-\delta_i\theta_i}\sin(\delta_i \ln r_i + \theta_{i0}), \quad i = n+1, \ldots, N,$$
$$\omega_i = 2a_i\pi\,\delta_i e^{-\delta_i\theta_i}\cos(\delta_i \ln r_i + \theta_{i0})\delta(x_i)\delta(y_i) \tag{25}$$

with arbitrary positive integers k, m, n, N, arbitrary constants a_i, δ_i, arbitrary functions $x_{i0} \equiv x_{i0}(t), y_{i0} \equiv y_{i0}(t)$, $i = 1, \ldots, N$, and $x_i \equiv x - x_{i0}, y_i \equiv y - y_{i0}$.

It has to be explained that the sources solutions (22)–(25) are weak solutions of the model. A weak solution of the model (5)–(6) means that it is an exact solution at all analytical areas. However, at the singular source points $\{x_i, y_i\}$, (22)–(25) will not result exact zero identities but the zero distributions. For instance, for the case both ψ_i and ψ_j are given by (23), the zero distributions, P_{ij}, read

$$\begin{aligned} P_{ij} = {} & \frac{4\pi a_i}{r_i^2}(y_i y_{i0t} + x_i x_{i0t})\left[\delta(x_i)\delta(y_i) + \ln(r_i)\Delta_i\right] - \frac{a_i^2\theta_i}{r_i^2}\left[3\delta(x_i)\delta(y_i) + \ln(r_i)\Delta_i\right] \\ & - \frac{a_i a_j}{r_i^2 r_j^2}\left[(x_i y_j - x_j y_i)\ln(r_i) + (x_i x_j + y_i y_j)\theta_i\right]\left[3\delta(x_j)\delta(y_j) + \ln(r_j)\Delta_j\right] \\ & + \frac{16\pi^2 a_i a_j C}{r_i^2 r_j^2}(x_i y_j - x_j y_i)\left[3\delta(x_i)\delta(y_i) + \ln(r_i)\Delta_i\right]\left[3\delta(x_j)\delta(y_j) + \ln(r_j)\Delta_j\right] \end{aligned} \tag{26}$$

where $\Delta_i \equiv x_i\delta'(x_i)\delta(y_i) + y_i\delta(x_i)\delta'(y_i)$ and $\delta'(x_i)$ is the derivative of the Dirac delta function with respect to its argument. We call P_{ij} zero distribution because

$$\int_{-\infty}^{+\infty}\int_{-\infty}^{+\infty} f(x, y)P_{ij}\mathrm{dxdy} = 0 \tag{27}$$

is satisfied for *arbitrary* function $f(x, y)$.

From (26), one can know that the sources (22)–(25) are really weak solutions of the models (5)–(6) no matter the VVI is involved or not. The only difference is that the zero distribution will have an additional term, say, the last term of (26).

The solutions (22)–(25) are all vortex source solutions. The first type expressed by Eq. (22) is well known in the literature [44] as the *point vortex source* similar to the magnetic line of an infinitely long wire.

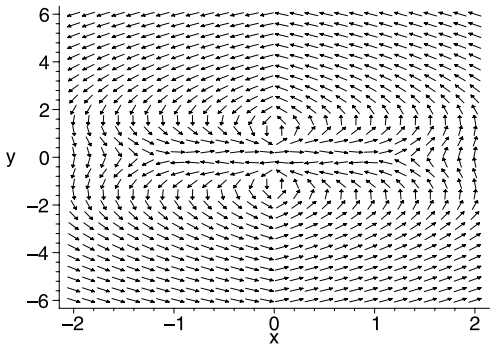

Fig. 1. A single vortex dipole structure of the EE with the stream function solution (28).

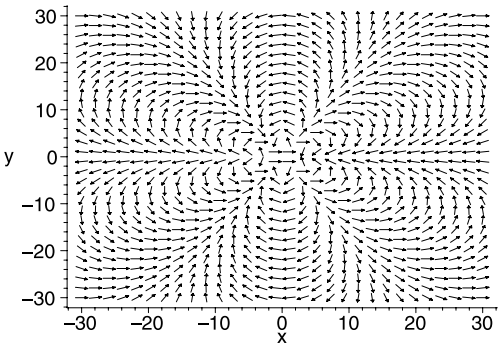

Fig. 2. A six-pole structure determined by Eq. (29).

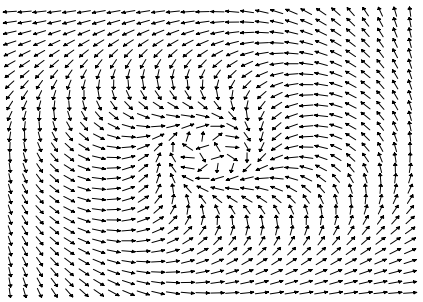

Fig. 3. The structure of a special negative cyclon for ψ_{1-} given in Eq. (30).

The solution (23) is related to the multiple *vortex dipole source* solution. Fig. 1 exhibits a single vortex dipole structure with the stream function

$$\psi_1 = \ln^2 r_1 - \theta_1^2, \qquad x_1 = y_1 = 0. \tag{28}$$

It is noted that to make the stream lines clearly, all the arrows in the figures in this paper have the same length except for Figs. 4 and 5.

The solution (24) is associated with the multiple vortex-like *multi-pole source* solution. For instance, $\delta_i = 2$ and 3 of Eq. (24) describe the single vortex quadruple and six-pole structures, respectively. Fig. 2 denotes a special six-pole structure with

$$\psi_1 = r_1^{-3} \sin(3\theta_1) = \frac{y(3x^2 - y^2)}{(x^2 + y^2)^3}, \qquad x_1 = y_1 = 0. \tag{29}$$

The solution (25) displays the structure of a *multiple cyclon* solution. We define a negative/positive cyclon as a vortex possessing a hole-like/source-like cycle. In other words, all the flows of a negative cyclon flow into the cycle, while flow out for a positive cyclon. Fig. 3 displays a special negative cyclon structure with a limit cycle in which the stream function reads

$$\psi_{1\mp} = \exp(\mp 2\theta) \sin(\ln(x^2 + y^2)), \qquad x_1 = y_1 = 0 \tag{30}$$

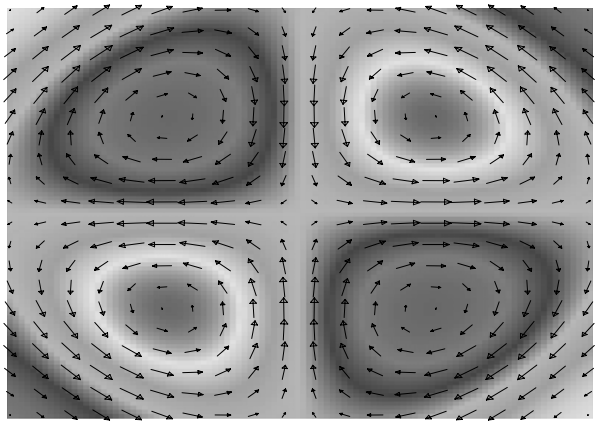

Fig. 4. The second BV with quadrupole structure (32) with $N = a_1 = C = 1, x_{i0} = y_{i0} = t = 0, c_1 = 2$.

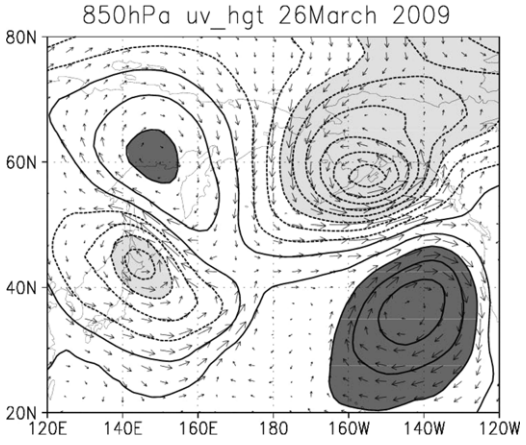

Fig. 5. Geopotential height (contour) and velocity (vector) fields at 850 hPa occurred on 26 March 2009.

for the up sign "−". The lower positive sign "+" is corresponding to a positive cyclon, which has a similar structure as displayed in Fig. 3 but with an opposite rotation.

It is interesting to mention that the axes and tick-marks are removed in Fig. 3 because this typical solution possesses a fractal structure. Concretely, if we plot the velocity field with the stream function (30) at the space regions

$$x = [-\alpha^n, \alpha^n], \qquad y = [-\alpha^n, \alpha^n], \quad \alpha \equiv e^{\pi}, \tag{31}$$

we can find the exactly same figures as shown in Fig. 3 for an arbitrary integer $n > 1$.

Positive and negative cyclons can be combined (say, $\psi_1 = \psi_{1+} + \psi_{1-}$) to produce various *cyclon dipole sources*.

4.2. Bessel vortices for $\beta \neq 0$ case

For the rotating fluid (nonzero β case), one can find the following type of *Bessel-vortex* (BV) solutions

$$\psi_i = a_i \sin(c_i\alpha_i + b_i) J_{c_i}(\rho_i/\sqrt{C}), \quad i = 1, \ldots, N \tag{32}$$

with the corresponding vorticities $\omega_i = -\psi_i/C$, where a_i, b_i, c_i are arbitrary constants, $J_{c_i}(x)$ is the c_i-th order Bessel function and C is just the strength constant of the VVI, and $\alpha_i = \arctan[(y-y_{i0})/(x-C\beta t+x_{i0})]$, $\rho_i = \sqrt{(x - C\beta t + x_{i0})^2 + (y - y_{i0})}$ with constants x_{i0}, y_{i0}.

To prove the correctness of (32) one can first introduce the moving coordinate $\{x' = (x - C\beta t + x_{i0}),\ y' = y - y_{i0}\}$, and then it is not difficult to find the result by using the variable separation approach under the polar coordinate.

The c_i-th BV denotes multi-pole vortex solutions which may be used to describe a variety of real phenomena in atmospheric and oceanic dynamics. For instance, the first BV ($c_i = 1$) is called modon. The concept modon is usually used to describe an atmospheric blocking which is responsible for some disasters such as the floods, drought, snow storm, etc. [46].

The 2nd BV is a quadrupole vortex solution as shown in Fig. 4 for $N = a_1 = C = 1, x_{i0} = y_{i0} = t = 0, c_1 = 2$. Similar vortex structures can be observed in the rotating fluids. Fig. 5 displays a saddle field in atmosphere occurred at mid-latitude

over the North Pacific on 26 March, 2009, appearing two cyclonic lows (light gray) and anticyclonic highs (heavy gray). Investigating the larger scale atmospheric circulation before and after this date, it is found that the 2nd BV pattern seems coming from a Rossby wave train at a sphere with strong synoptic eddies traveling split northward and southward before an atmospheric blocking formed.

5. Characteristic features of vortex interactions under the MVIM without the β-effect

By this far we have studied the analytical properties of the MVIM. In this section, we go further to show that some observed patterns of the atmospheric vortex interactions can be derived from the numerical results of the MVIM. We do not consider the β effect here, since the barotropic vorticity equation with finite beta does not have stationary monopolar vortex solutions as demonstrated in several papers.

In our numerical simulations, the initial profile of vortex is given by

$$\psi = y_{0t}x - x_{0t}y - A\left(2 + 2\frac{r}{r_m} + \frac{r^2}{r_m^2}\right)e^{-\frac{r}{r_m}}, \tag{33}$$

where $r = \sqrt{(x-x_0)^2 + (y-y_0)^2}$. x_0 and y_0 are arbitrary functions of t, which denote the central position of the vortex at time t. This vortex is first used to describe the shape of a tropical cyclone (TC) and the tract of the TC eye in a pioneering work [24]. In [47], the author explains the variety of tracks of TC based on a mathematical model. The absolute value of A denotes the intensity of the vortex, and if A is positive, the vortex is anti-clockwise (TC in the northern hemisphere); if A is negative, the vortex is clockwise (TC in the southern hemisphere). r_m is a positive constant that controls the radius of the vortex. The size of the vortex increases as r_m is getting larger. The first two terms on the right-hand-side of (33) represent the background flow in which the vortex is embedded. If the background flow is eliminated, a pure vortex can be obtained as

$$\psi = -A\left(2 + 2\frac{r}{r_m} + \frac{r^2}{r_m^2}\right)e^{-\frac{r}{r_m}}. \tag{34}$$

The expression (33) is an exact solution of the $(2+1)$-dimensional Euler equation, which is obtained via the symmetry group transformation method [24]. Here we neglect the influence of background flow and use expression (34) as initial condition.

In Fig. 6 we depict the evolution of the stream function of a single vortex form $t = 0$ to $t = 1000$. The lines denote the contours of the stream function, and the heavier the line's color is, the smaller the height is. The direction of an arrow denotes the direction of the velocity of the stream at that point, while the length of the arrow denotes the absolute value of the velocity. (The meanings of the contour lines and arrows are the same for the following figures in this work.) It shows clearly that if there are no outside influences, the vortex can keep its shape for a very long time. All the numerical simulations in this paper are implemented via the PDE-module of the finite element software COMSOL multiphysics 3.5.

5.1. Interactions between two equal vortices

An intensive investigation of the interactions between two vortices is a groundwork for further studies which involves more vortices. From the MVIM mentioned in Section 1, a binary vortex interaction model (BVIM) can be derived as

$$\begin{aligned}
&\omega_1 = \Delta\psi_1,\\
&\omega_{1t} + [\psi_1, \omega_1] + [\psi_1, \omega_2] + C[\omega_1, \omega_2] = 0,\\
&\omega_2 = \Delta\psi_2,\\
&\omega_{2t} + [\psi_2, \omega_2] + [\psi_2, \omega_1] + C[\omega_2, \omega_1] = 0,
\end{aligned} \tag{35}$$

where Δ is the two-dimensional Laplacian, and β has been chosen as zero.

First, we study interactions between two equal vortices

$$\psi_1 = -A\left(2 + 2\frac{r_1}{r_m} + \frac{r_1^2}{r_m^2}\right)e^{-\frac{r_1}{r_m}}, \tag{36}$$

$$\psi_2 = -A\left(2 + 2\frac{r_2}{r_m} + \frac{r_2^2}{r_m^2}\right)e^{-\frac{r_2}{r_m}}, \tag{37}$$

where $r_1 = \sqrt{(x-x_{10})^2 + (y-y_{10})^2}$, $r_2 = \sqrt{(x-x_{20})^2 + (y-y_{20})^2}$. The two vortices have the same radius and intensity, and they spin in the same direction, yet their initial positions are different.

In numerical simulations, we find that there exists a *separation distance*, which is an important threshold for the binary interaction behavior. If the distance between the centers of the two vortices is smaller than the separation distance, the two vortices will begin orbiting around each other, and gradually combine. At last, they merge into a single vortex which has larger size. If the distance between the centers of the two vortices is larger than the separation distance, they will separate.

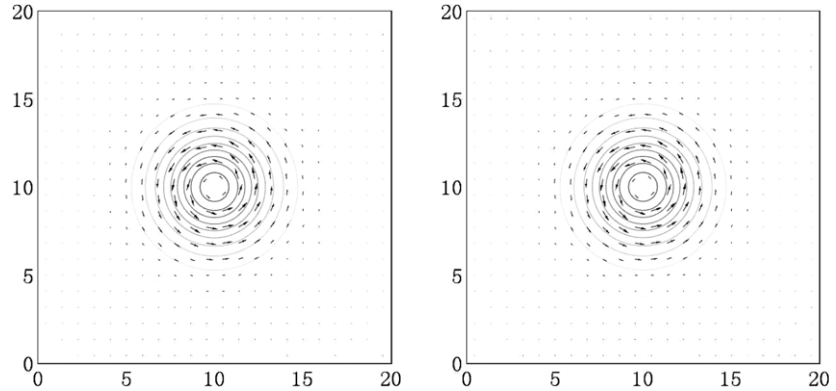

(a) $t = 0$. (b) $t = 1000$.

Fig. 6. Evolution of a single vortex (34) with $x_0 = y_0 = 10, A = 1, r_m = 1$. The vortex keeps its shape without outside influences. The lines denote the contours of the stream function, and the heavier the line's color is, the smaller the height is. The direction of an arrow denotes the direction of the velocity of the stream at that point, while the length of the arrow denotes the absolute value of the velocity. (The meanings of the contour lines and arrows are the same for the following figures in this work.)

During the separation, they keep orbiting around each other and, the angular velocity of their movement decreases as the distance between their centers increases. Finally, the two vortices will stop orbiting each other. Actually, if the initial distance between the centers of the two vortices is large enough, the interactions between them can be completely neglected. This fact shows that the binary vortex interactions implied in the BIVM are local, not global. We also find that if the self-rotation of the two vortices is anti-clockwise, their mutual orbiting movement is also anti-clockwise.

The separation distance is related to the size and the intensity of each vortex. In simulations, we find that the separation distance increases as the radius of each vortex increases. The effects of intensity are similar to that of the radius, yet it is less obvious. So we conjecture that the separation distance mainly relates to the influential range of each vortex.

We also find that the coefficient C in the BIVM (35) has very small influence on the binary interaction behaviors. This fact suggests that the stream–vorticity interactions dominated the interaction patterns. So the high order nonlinear effects, that is, the vorticity–vorticity interactions, can be neglected in the BIVM when the vortices do not overlap.

In Fig. 7, the evolution of an initial configuration given by (36)–(37) is depicted, where we have set $A = r_m = 1, x_{10} = 27.2, x_{20} = 33$ and $y_{10} = y_{20} = 30$. Under this setting, the initial distance between the centers of the two vortices is 5.8. It can be seen that, the two vortices at first orbit around each other, then combine, and finally merge. A new vortex with larger size and intensity is generated. For the second simulation, we set $x_{10} = 27$ and keep all other parameters invariable. In this case, the initial distance between the centers of the two vortices is 6, which is larger than that in the first simulation. This time, the two vortices separate, which can be seen clearly in Fig. 8. The evolution also shows that the two vortices are mutually orbiting around each other anti-clockwise during the separation, while each vortex spins anti-clockwise. Meanwhile, the angular velocity of their mutual orbiting is decreasing. It can be seen that from $t = 0$ (Fig. 8(a)) to $t = 40$ (Fig. 8(d)) the rotation of each vortex around their centroid is almost 90°, while from $t = 60$ (Fig. 8(e)) to $t = 100$ (Fig. 8(f)) the rotation is trivial. From the first two simulations we conjugate that the separation distance of the two vortices (36)–(37) with $A = r_m = 1$ is between 5.8 and 6.

The third simulation is depicted in Fig. 9, in which the initial distance between the centers of the two vortices is 10. The corresponding x-positions are $x_{10} = 25, x_{20} = 35$, and all other parameters are unchanged. The evolution of the initial configuration shows that when the initial distance between two vortices is larger, the interactions between them are very weak. The separation velocity of the two vortices is slow and, the angular velocity of their mutual orbiting is also less than that observed in the second simulation.

For the fourth simulation in this section, we show that the separation distance depends on the size of each vortex. In Fig. 10, we show the evolution of two larger vortices, with $r_m = 1.75, A = 1, x_{10} = 25, x_{20} = 35$ and $y_{10} = y_{20} = 30$. The initial distance between these two vortices is 10. In Fig. 9, we show that under this initial distance vortices having smaller radius display very weak binary interactions, yet two larger vortices do emerge as it is depicted in Fig. 10. Similarly, the intensity of each vortex will also affect the separation distance. If the intensity is reduced for each vortex, their binary interaction will become weaker. In this case, the separation distance will be smaller.

Our numerical results are well consistent with some known phenomena in meteorology, introduced by a lot of experiments, observations and theoretical studies that described the binary interaction between two tropical cyclones. The most obvious phenomenon exhibited in all these four simulations is the mutual orbiting, that is the famous Fujiwhara effect. Since it was first revealed by fluid mechanics experiments in water tank [26], the Fujiwhara effect has been developed to be a central concept which describes the interactions of binary tropical cyclones. In the western North Pacific typhoon season, the Fujiwhara effect happens frequently between two typhoons owing to the greater number of tropical cyclones there. The Fujiwhara effect also happens between two hurricanes in the eastern North Pacific or in the North Atlantic. In Fig. 11,

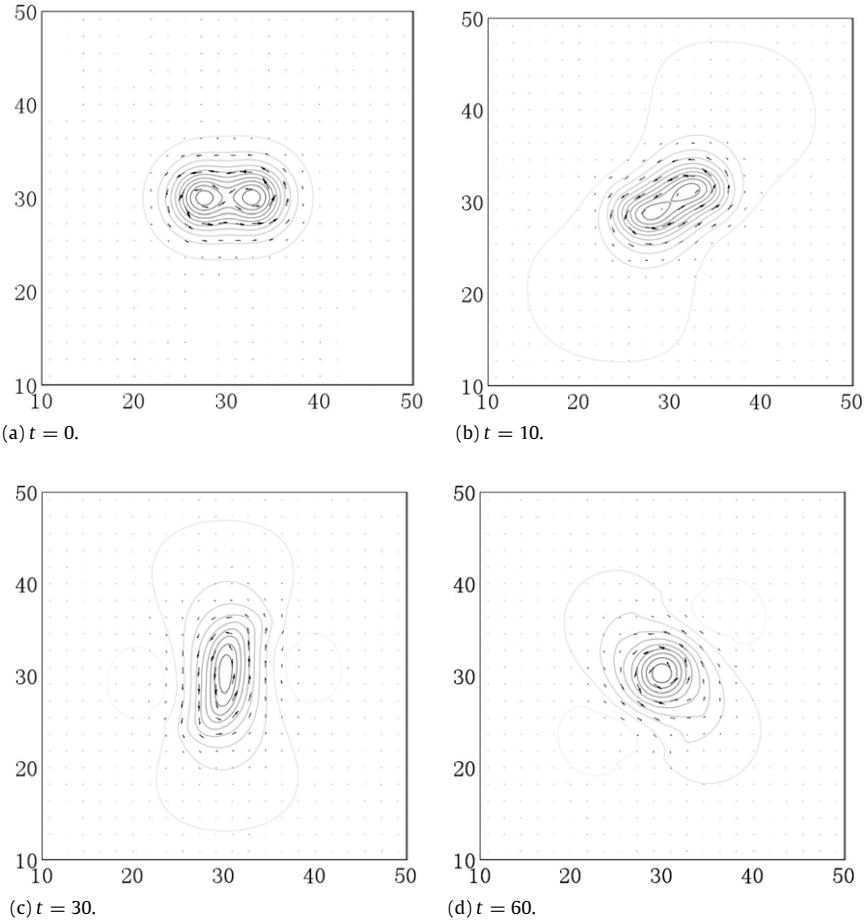

(a) $t = 0$. (b) $t = 10$.

(c) $t = 30$. (d) $t = 60$.

Fig. 7. Evolution of two vortices (36) and (37) with $x_{10} = 27.2$, $x_{20} = 33$, $y_{10} = y_{20} = 30$, $A = 1$, $r_m = 1$. The coefficient C in the BIVM (35) is set to 1. The two vortices gradually merge in this case.

the satellite image of two interacting hurricanes is shown, where Hurricane Ione (left) and Hurricane Kirsten (right) are displaying the Fujiwhara effect at August 24, 1974. The image is downloaded from the web given in [48].

In Ref. [49], Lander and Holland made a detailed analysis of the observed behavior of interacting cyclonic vortices in the western North Pacific region. Besides the classical Fujiwhara effect, they pointed out that a series of interactions including cyclone merging and escaping take place during the interaction of cyclones. They showed that there exists a threshold distance (which is called separation distance in their work) for the interactions of cyclones. If the distance between two cyclones is smaller than the separation distance, they tend to combine, or they will escape from each other. The numerical results of our BIVM models in this section are well consistent with their analysis. We also show that the separation distance relates to the size and intensity of each vortex.

5.2. Interactions between two nonequal vortices

Now we study the binary interactions between two nonequal vortices

$$\psi_1 = -A_1 \left(2 + 2\frac{r_1}{r_{m1}} + \frac{r_1^2}{r_{m1}^2}\right) e^{-\frac{r_1}{r_{m1}}}, \tag{38}$$

$$\psi_2 = -A_2 \left(2 + 2\frac{r_2}{r_{m2}} + \frac{r_2^2}{r_{m2}^2}\right) e^{-\frac{r_2}{r_{m2}}}, \tag{39}$$

where $r_1 = \sqrt{(x - x_{10})^2 + (y - y_{10})^2}$, $r_2 = \sqrt{(x - x_{20})^2 + (y - y_{20})^2}$. The two vortices have different radiuses and intensities, which are controlled by r_{mi} and A_i $(i = 1, 2)$ respectively.

Basically, the binary interactions of two nonequal vortices are similar to that of two equal ones. The interaction behaviors such as merging, mutual orbiting and separation also exist. However, these behaviors will be affected to some degree as the

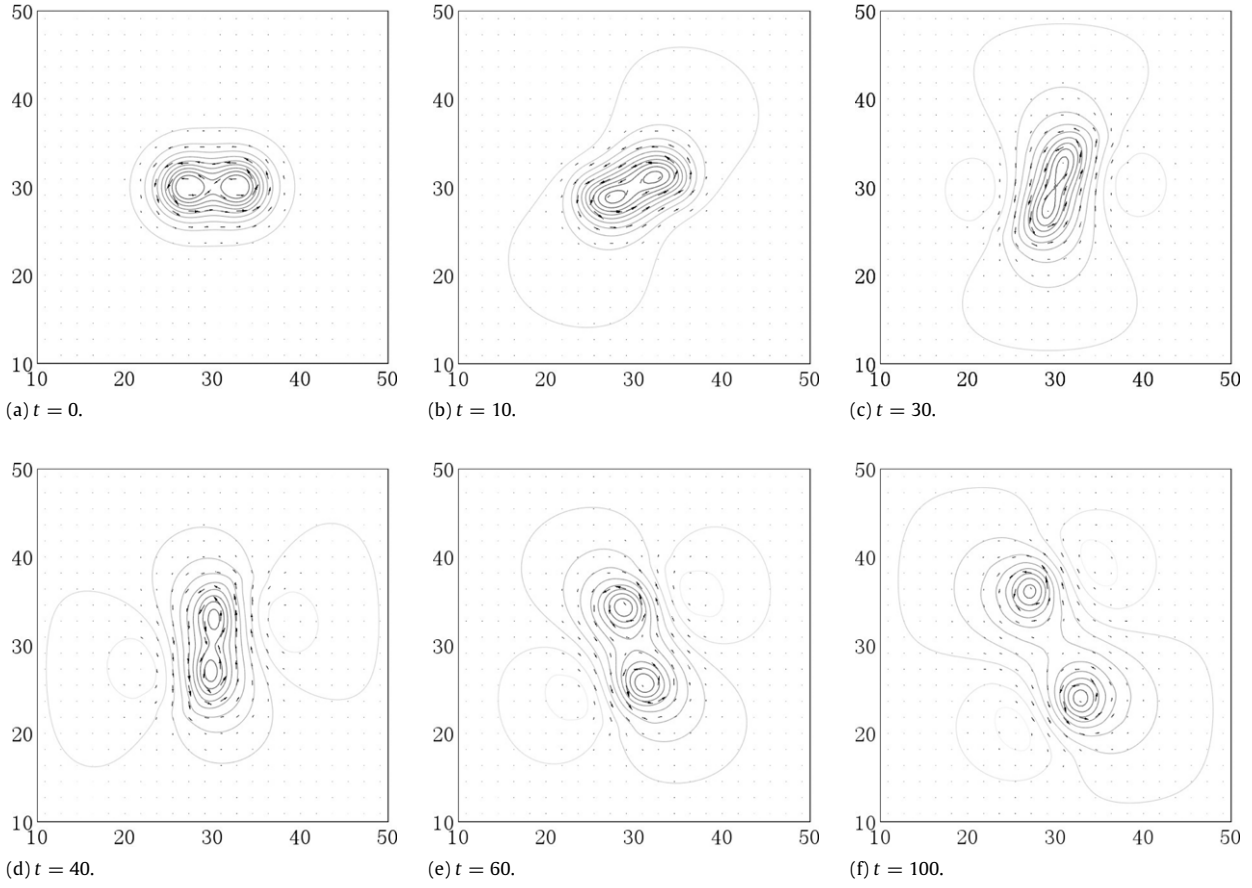

Fig. 8. Evolution of two vortices (36) and (37) with $x_{10} = 27$, $x_{20} = 33$, $y_{10} = y_{20} = 30$, $A = 1$, $r_m = 1$. The coefficient C in the BIVM (35) is set to 1. The two vortices separate in this case.

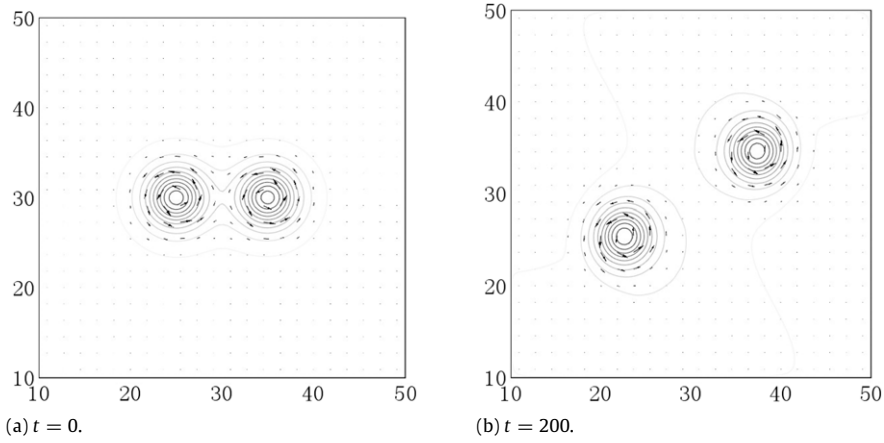

Fig. 9. Evolution of two vortices (36) and (37) with $x_{10} = 25$, $x_{20} = 35$, $y_{10} = y_{20} = 30$, $A = 1$, $r_m = 1$. The coefficient C in the BIVM (35) is set to 1. The binary vortex interaction is weak.

two vortices are different in a few aspects, and new interaction patterns thus emerge. An easily observed interaction pattern is *absorption*, which usually happens between two vortices with different intensities.

In Fig. 12 the evolution of an initial configuration given by (38)–(39) is depicted, where we have set $x_{10} = 25$, $x_{20} = 35$, $y_{10} = y_{20} = 30$, $A_1 = 1$, $A_2 = 2/3$ and $r_{m1} = r_{m2} = 1.75$. Under this setting, the two vortices have the same size, the initial distance between their centers is 10, and the intensity ratio is 1.5. It can be seen clearly that the vortex with smaller intensity is absorbed into the one with larger intensity. This kind of absorption can also happen between two vortices with different sizes. For the second simulation, we set $x_{10} = 25$, $x_{20} = 35$, $y_{10} = y_{20} = 30$, $A_1 = 1$, $A_2 = 0.5$, $r_{m1} = 1$, $r_{m2} = 2$.

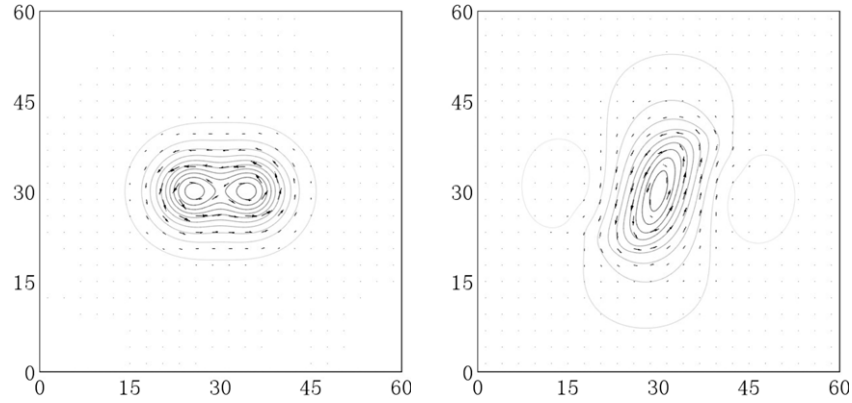

(a) $t = 0$. (b) $t = 75$.

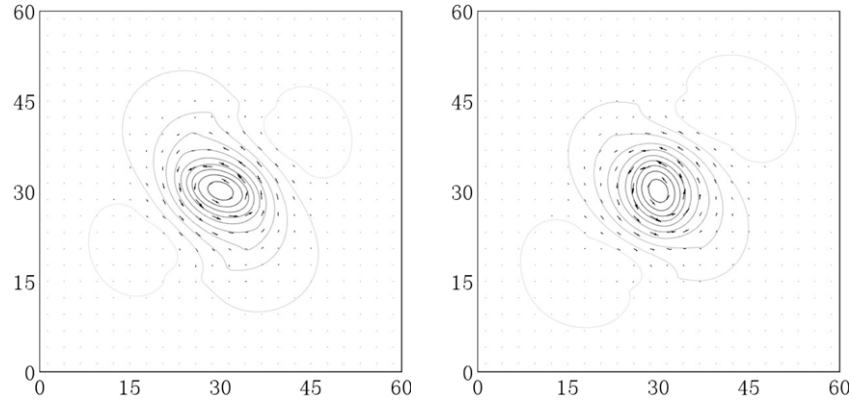

(c) $t = 150$. (d) $t = 200$.

Fig. 10. Evolution of two vortices (36) and (37) with $x_{10} = 25$, $x_{20} = 35$, $y_{10} = y_{20} = 30$, $A = 1$, $r_m = 1.75$. The coefficient C in the BIVM (35) is set to 1. The separation distance increases as the size of each vortex increases.

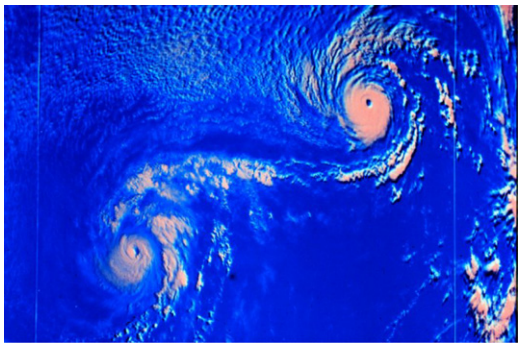

Fig. 11. Hurricane Ione (left) and Hurricane Kirsten (right) are displaying the Fujiwhara effect at August 24, 1974.

From the evolution depicted in Fig. 13 we can see that the smaller vortex is strengthened and enlarged while the larger one gradually shrank. According to this, we suppose that the process of absorption is mainly dominated by the vortex with larger intensity. The absorption of a weaker cyclone into a stronger one is also observable in meteorology. For example, a tropical cyclone was absorbed by Hurricane Lisa in 2004, which has been described in the Tropical Cyclone Report [50].

5.3. Interactions between a cyclonic vortex and an anticyclonic vortex

By far we are confined to interactions of two vortices spinning in the same direction. It is also an important issue to investigate interactions of two vortices which spin in different directions. In the northern hemisphere, a cyclonic vortex

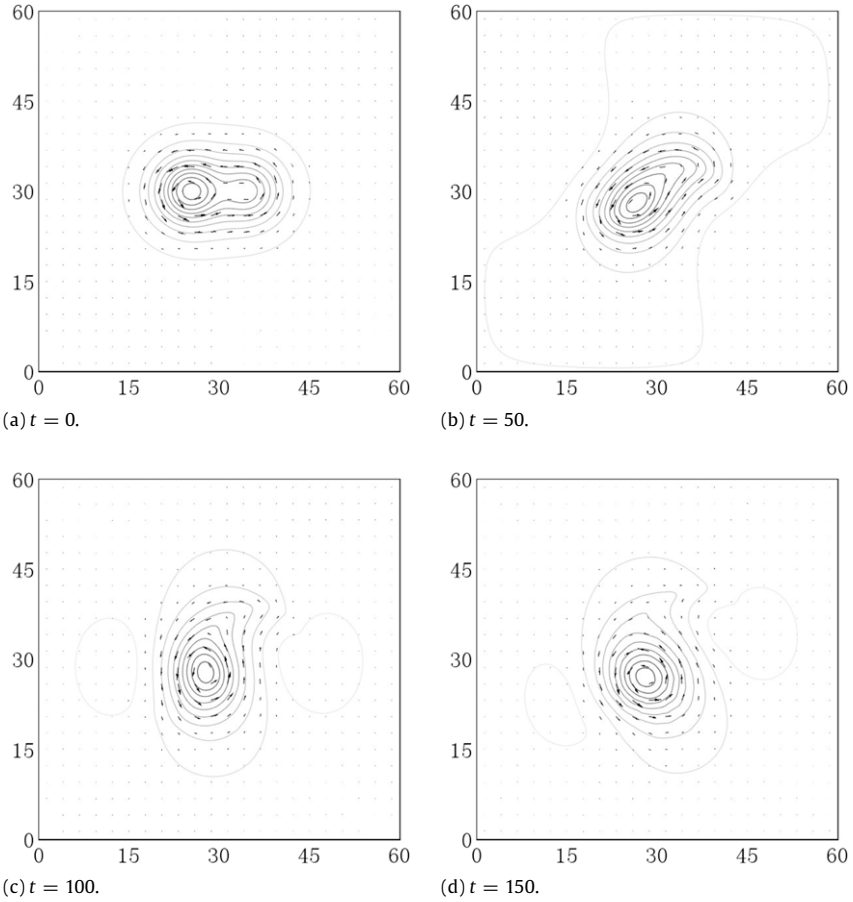

Fig. 12. Evolution of two nonequal vortices (38) and (39) with $x_{10} = 25, x_{20} = 35, y_{10} = y_{20} = 30, A_1 = 1, A_2 = 2/3, r_{m1} = r_{m2} = 1.75$. The coefficient C in the BIVM (35) is set to 1. The vortex with smaller intensity is absorbed into the one with larger intensity.

spins anticlockwise, while an anticyclonic vortex spins clockwise. It is a crucial problem to study interactions between a cyclone and an anticyclone in meteorology, owing to the high possibility of this kind of interactions. For example, a typhoon (cyclonic vortex) in the western North Pacific is often affected by a subtropical high (anticyclonic vortex). Now we move on to study the interactions between a cyclonic vortex and an anticyclonic vortex.

In Fig. 14 we show the effect of a subtropical high on a cyclonic vortex. We use a large vortex spinning clockwise to denote the subtropical high in the northern hemisphere. Its mathematical expression is given by (38) with $x_{10} = 40$, $y_{10} = 40, A_1 = -1, r_{m1} = 3$. The small vortex spinning anticlockwise denotes the cyclone, which is given by (39) with $x_{20} = 55, y_{20} = 25, A_2 = 1, r_{m2} = 1$. The cyclone locates at the lower right of the subtropical high. This is the normal situation in the northwest Pacific, which is a famous typhoon-prone area. It can be seen from the evolution that the cyclone orbit around the subtropical high clockwise and is weakened during the orbiting. At the same time, the subtropical high is jostled by the cyclone and distorted. In Fig. 15 the tracks of Hurricane Ioke (2006) and Typhoon Tip (1979) are depicted. (The images are downloaded from the web [51] and [52] respectively.) The anticlockwise tracks are similar to the path of the cyclonic vortex shown in Fig. 14.

6. Summary and discussions

In summary, some multiple vortex interaction models (5)–(6) with and without VVI are established for an inviscid nondissipative and equivalent barotropic vorticity system in a beta-plane channel. It is found that the models with SVI but without VVI possess more abundant symmetries and CLs than those with both VVI and SVI. It is demonstrated that the SVI preserves the self-energy of every vortex and the interaction energy of every two vortices while destroys the enstrophy CLs for every vortex. However, the VVI destroys both the energy CLs and the enstrophy CLs for every single vortex.

Some nontrivial exact vortices and vortex source solutions are obtained for both the $\beta = 0$ and $\beta \neq 0$ cases. In detail, some multiple point vortex source solutions, multiple vortex dipole sources, multiple vortex multi-pole source solutions,

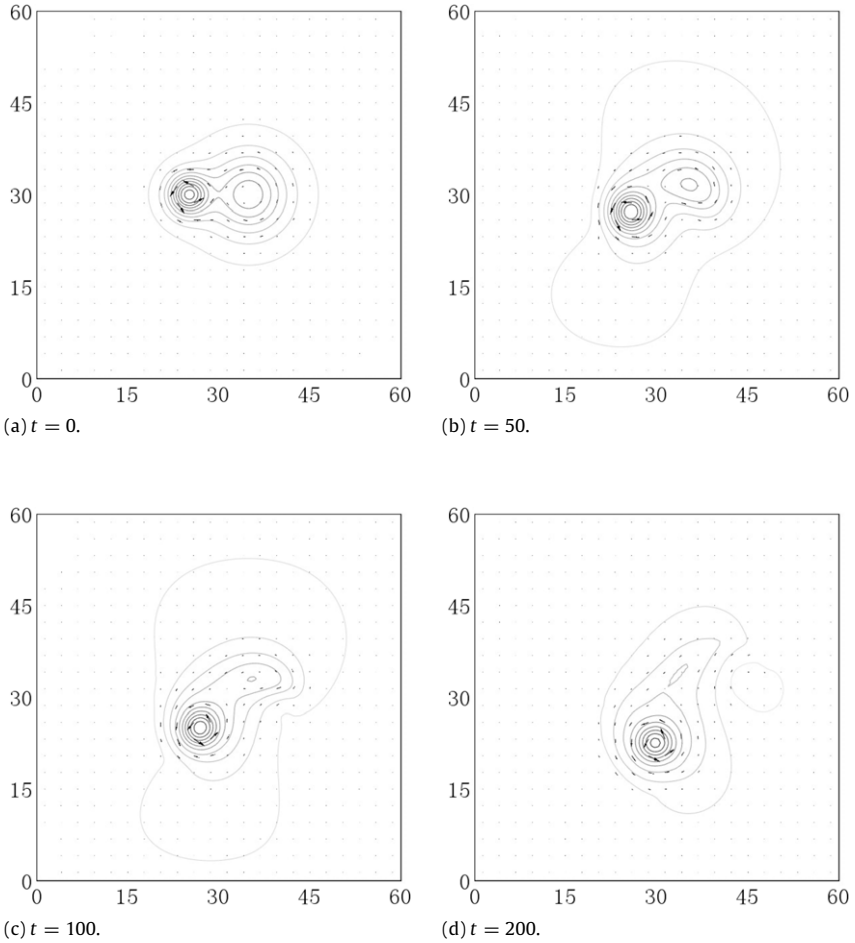

(a) $t = 0$. (b) $t = 50$.

(c) $t = 100$. (d) $t = 200$.

Fig. 13. Evolution of two nonequal vortices (38) and (39) with $x_{10} = 25, x_{20} = 35, y_{10} = y_{20} = 30, A_1 = 1, A_2 = 1/2, r_{m1} = 1, r_{m2} = 2$. The coefficient C in the BIVM (35) is set to 1. The larger vortex is absorbed by the smaller one.

multiple fractal cyclons, multiple fractal cyclon dipoles and Bessel vortices are obtained. To our knowledge the multi-pole source solutions, fractal cyclon source solutions, fractal cyclon dipole sources and *arbitrary order* BV have not yet been found before. Since there exist various vortices in real nature, it is hoped that all the vortex solutions presented above might be observed from the real natural phenomena, or from fluid experiments and other physical fields. Here, a special 2nd BV observation of a circulation pattern occurred over the North Pacific on 26 March 2009 is offered.

By using the numerical approach, the characteristic features of vortex interactions are discussed under the MVIM without the β-effect. For two equal vortices, we find out that there exists a separation distance which is a threshold for the interaction behaviors. Two vortices tend to combine and merge when the distance between their centers is smaller than their separation distance, or else they separate from each other. During the merging or separation, the two vortices mutually orbit around each other. These interaction behaviors are well consistent with a lot of known observations for cyclonic vortices in meteorology. We also investigate interactions between nonequal vortices and identify two kinds of intensity dominated absorption, where the vortex with smaller intensity is absorbed into the one with larger intensity. Next we explore the interactions between a cyclonic vortex and a subtropical high in the northern hemisphere. The numerical results show that the cyclonic vortex tends to orbit the subtropical high clockwise, while the subtropical high is jostled by the cyclone and distorted. Those characteristic features of vortex interactions are compared with some known results of fluid mechanical experiments and meteorologic observations.

Though the multiple vortex interaction models with both the SVI and VVI are established, and some special exact vortex and vortex source solutions are obtained, many important problems are still open. For instance, are there any useful Lax pairs for the MVIM? How to find exact vortex source solutions of the model for $\beta \neq 0$? How to explore exact multiple *analytical* non-source solutions for $\beta = 0$? How to discover any other types of multiple vortex solutions responsible for the hurricanes or other disastrous weather? How to modify the MVIM (5)–(6) further to study other possible structures and interactions of the multiple vortices?

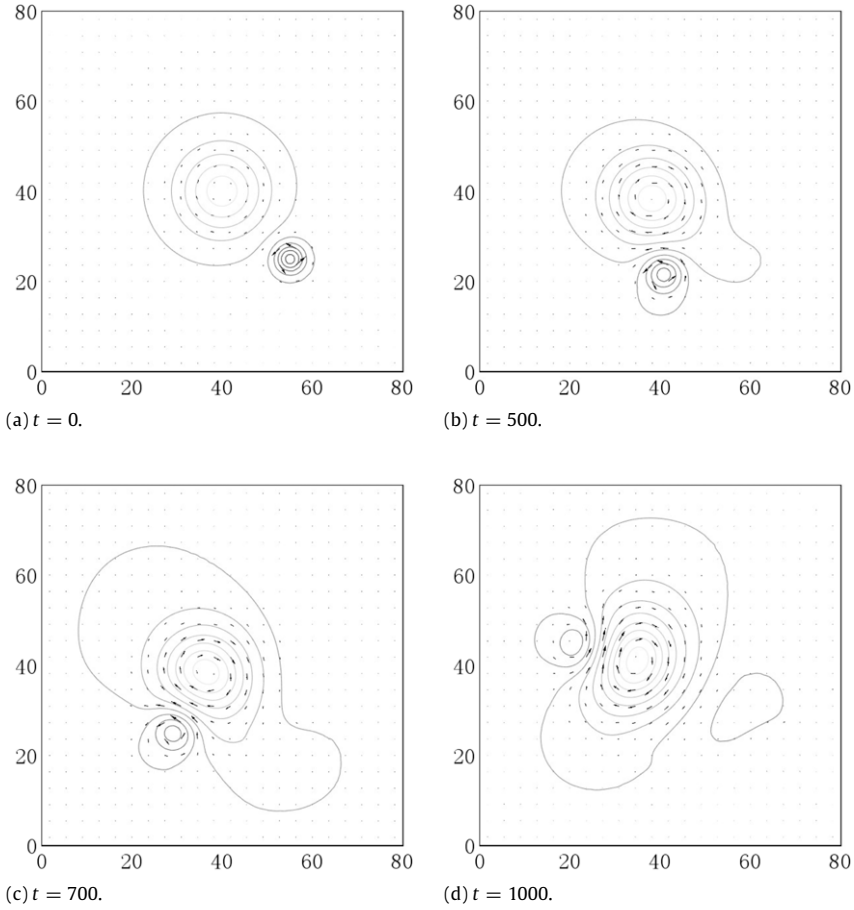

Fig. 14. Evolution of two nonequal vortices (38) and (39) with $x_{10} = 40, x_{20} = 55, y_{10} = 40, y_{20} = 25, A_1 = -1, A_2 = 1, r_{m1} = 3, r_{m2} = 1$. The coefficient C in the BIVM (35) is set to 1. The larger anti-vortex denotes a subtropical high, while the smaller vortex denotes a cyclonic vortex.

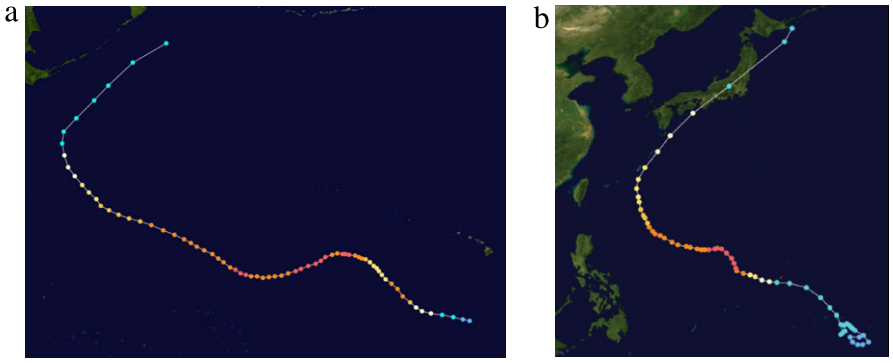

Fig. 15. The tracks of Hurricane Ioke (a) and Typhoon Tip (b).

Acknowledgments

The work was sponsored by the National Natural Science Foundation of China (Nos. 11175092 and 10735030) and the National Basic Research Programs of China (973 Programs 2007CB814800). The authors are sponsored by K.C. Wong Magna Fund in Ningbo University.

References

[1] P.G. Saffman, Vortex Dynamics, Cambridge University Press, 1992.
[2] E.K. Dahl, E. Babaev, A. Sudbø, Unusual states of vortex matter in mixtures of Bose–Einstein condensates on rotating optical lattices, Phys. Rev. Lett. 101 (2008) 255301;
M. Abad, M. Guilleumas, R. Mayol, M. Pi, D.M. Jezek, Vortices in Bose–Einstein condensates with dominant dipolar interactions, Phys. Rev. A 79 (2009) 063622.
[3] N.K. Efremidis, K. Hizanidis, B.A. Malomed, P.D. Trapani, Three-dimensional vortex solitons in self-defocusing media, Phys. Rev. Lett. 98 (2007) 113901;
S.H. Chen, J.M. Dudley, Spatiotemporal nonlinear optical self-similarity in three dimensions, Phys. Rev. Lett. 102 (2009) 233903.
[4] H. Li, J.R. Friend, L.Y. Yeo, Microfluidic colloidal Island formation and erasure induced by surface acoustic wave radiation, Phys. Rev. Lett. 101 (2008) 084502;
D.G. Thomas, R. Sureshkumar, B. Khomami, Pattern formation in Taylor–Couette flow of dilute polymeric solutions: dynamical simulations and mechanism, Phys. Rev. Lett. 97 (2006) 054501.
[5] T.N. Jukes, K.S. Choi, Long lasting modifications to vortex shedding using a short plasma excitation, Phys. Rev. Lett. 102 (2009) 254501;
T.K. Nakamura, M. Fujimoto, Magnetic effects on the coalescence of Kelvin–Helmholtz vortices, Phys. Rev. Lett. 101 (2008) 165002;
D. Sundkvist, S.D. Bale, Characteristic parameters of drift vortices coupled to Alfvén waves in an inhomogeneous space plasma, Phys. Rev. Lett. 101 (2008) 065001.
[6] A. Penzev, Y. Yasuta, M. Kubota, AC vortex-dependent torsional oscillation response and onset temperature τ_0 in solid ^{4}He, Phys. Rev. Lett. 101 (2008) 065301.
[7] U.A. Dyudina, A.P. Ingersoll, S.P. Ewald, et al., Dynamics of Saturn's south polar vortex, Science 319 (2008) 1801;
F.T. Muijres, L.C. Johansson, R. Barfield, et al., Leading-edge vortex improves lift in slow-flying bats, Science 319 (2008) 1250–1253.
[8] J.R. Colantonio, J. Vermot, D. Wu, et al., The dynein regulatory complex is required for ciliary motility and otolith biogenesis in the inner ear, Nature (London) 457 (2009) 205–209;
A. Amo, D. Sanvitto, F.P. Laussy, et al., Collective fluid dynamics of a polariton condensate in a semiconductor microcavity, Nature (London) 457 (2009) 291–295.
[9] G. Yossifon, H.C. Chang, Selection of nonequilibrium overlimiting currents: universal depletion layer formation dynamics and vortex instability, Phys. Rev. Lett. 101 (2008) 254501.
[10] A. Tychensky, X.J. Carton, Hydrological and dynamical characterization of Meddies in the Azores region: a paradigm for baroclinic vortex dynamics, J. Geophys. Res. 103 (1998) 25061–25079.
[11] G. Brunet, M.T. Montgomery, Vortex Rossby waves on smooth circular vortices part I. Theory, Dyn. Atmos. Oceans 35 (2002) 153–177.
[12] S. Zhang, Z.H. Liu, Zh.G. Lin, Global minimizers of coexistence for rotating-component Bose–Einstein condensates, Nonlinear Anal. Real World Appl. 12 (2011) 2567–2578.
[13] H.O. Äkerstedt, J. Nycander, V.P. Pavlenko, Three-dimensional stability of drift vortices, Phys. Plasmas 3 (1996) 160–167.
[14] L.P. Graves, J.C. McWilliams, M.T. Montgomery, Vortex evolution due to straining: a mechanism for dominance of strong, interior anticyclones, Geophys. Astrophys. Fluid Dyn. 100 (2006) 151–183.
[15] V.M. Canuto, M.S. Dubovikov, Modeling mesoscale eddies, Ocean Model. 8 (2005) 1–8.
[16] C. Girard, R. Benoit, M. Desgagne, Finescale topography and the MC2 dynamics kernel, Mon. Weather Rev. 133 (2005) 1463–1477.
[17] L. Faddeev, A.J. Niemi, U. Wiedner, Glueballs, closed fluxtubes, and eta(1440), Phys. Rev. D 70 (2004) 114033.
[18] A.J. Leggett, Bose–Einstein condensation in the alkali gases: some fundamental concepts, Rev. Modern Phys. 73 (2001) 307–356.
[19] I. Chuang, R. Durrer, N. Turok, B. Yurke, Cosmology in the laboratory: defect dynamics in liquid crystals, Science 251 (1991) 1336–1342.
[20] M.J. Bowick, L. Chandler, E.A. Schiff, A.M. Srivastava, The cosmological Kibble mechanism in the laboratory: string formation in liquid crystals, Science 263 (1994) 943–945.
[21] E. Babaev, A. Sudbø, N.W. Ashcroft, A superconductor to superfluid phase transition in liquid metallic hydrogen, Nature (London) 431 (2004) 666–668.
[22] K. Emanuel, Increasing destructiveness of tropical cyclones over the past 30 years, Nature (London) 436 (2005) 686–688.
[23] Q.H. Zhang, S.J. Chen, Y.H. Kuo, R.A. Anthes, Numerical study of a typhoon with a large eye: model simulation and verification, Mon. Weather Rev. 133 (2005) 725–742.
[24] S.Y. Lou, M. Jia, X.Y. Tang, F. Huang, Vortices, circumfluence, symmetry groups, and Darboux transformations of the (2+1)-dimensional Euler equation, Phys. Rev. E 75 (2007) 056318.
[25] F. Huang, X.Y. Tang, S.Y. Lou, C.H. Lu, Evolution of dipole-type blocking life cycle: analytical diagnoses and observations, J. Atmospheric Sci. 64 (2007) 52–73.
[26] S. Fujiwhara, The natural tendency towards symmetry of motion and its application as a principle of motion, Q. J. R. Meteorol. Soc. 47 (1921) 287–293.
[27] J.C. McWilliams, The emergence of isolated, coherent vortices in turbulent flow, J. Fluid Mech. 146 (1984) 21–43;
J.C. McWilliams, The vortices of two-dimensional turbulence, J. Fluid Mech. 219 (1990) 361–385.
[28] D.G. Dritschel, A general theory for two-dimensional vortex interactions, J. Fluid Mech. 293 (1995) 269–303.
[29] K.S. Fine, C.F. Driscoll, J.H. Malmberg, et al., Measurements of symmetric vortex merger, Phys. Rev. Lett. 67 (1991) 588–591;
T.B. Mitchell, C.F. Driscoll, Electron vortex orbits and merger, Phys. Fluids 8 (1996) 1828–1841.
[30] E.J. Hopfinger, G.J.F. van Heijst, Vortices in rotating fluids, Annu. Rev. Fluid Mech. 25 (1993) 241–289.
[31] J.J. Rasmussen, A.H. Nielsen, V. Naulin, Dynamics of vortex interactions in two-dimensional flows, Phys. Scr. T98 (2002) 29–33.
[32] M.V. Melander, N.J. Zabusky, J.C. McWilliams, Symmetric vortex merger in two dimensions, J. Fluid Mech. 195 (1988) 303–340.
[33] E. Lorin, A. Bandrauk, A simple and accurate mixed P^0-Q^1 solver for the Maxwell–Dirac equations, Nonlinear Anal. Real World Appl. 12 (2011) 190–202.
[34] F.G. Mitri, G.T. Silva, Off-axial acoustic scattering of a high-order Bessel vortex beam by a rigid sphere, Wave Motion 48 (2011) 392–400.
[35] A.J. Clark, W.A. Gallus, M. Xue, F. Kong, Convection-allowing and convection-parameterizing ensemble forecasts of a mesoscale convective vortex and associated severe weather environment, Weather and Forecasting 25 (2010) 1052–1081.
[36] Le Xuan Truong, Le Thi Phuong Ngoc, Cao Huu Hoa, Nguyen Thanh Long, On a system of nonlinear wave equations associated with the helical flows of Maxwell fluid, Nonlinear Anal. Real World Appl. 12 (2011) 3356–3372.
[37] Jorge Luis Domnguez Rodrguez, Mark Thompson, A balanced atmospheric model of Lorenz, Nonlinear Anal. Real World Appl. 11 (2010) 3251–3271.
[38] R. Koenig, Tornado rips apart Maryland center, Science 294 (2001) 284–285.
[39] D.J. Williams, W.T. Potter, W.W. Clarkson, et al., The impact of background ozone on compliance with revised national ambient air quality standards, J. Air Waste Manage. Assoc. 59 (2009) 52–57.
[40] B. Schaeler, D. Offermann, V. Kuell, et al., Global water vapour distribution in the upper troposphere and lower stratosphere during CRISTA 2, Adv. Space Res. 43 (2009) 65–73.
[41] S. Erard, P. Drossart, G. Piccioni, Multivariate analysis of visible and infrared thermal imaging spectrometer (VIRTIS) venus express nightside and limb observations, J. Geophys. Res. (Planets) 114 (2009) E00B27.
[42] K. Dong, C.J. Neumann, On the relative motion of binary tropical cyclones, Mon. Weather Rev. 111 (1983) 945–953.
[43] J. Pedlosky, Geophysical Fluid Dynamics, Springer-Verlag, 1979.
[44] H. Lamb, Hydrodynamics, sixth ed., Dover, New York, 1945;
S.Y. Lou, M. Jia, F. Huang, X.Y. Tang, Bäcklund transformations, solitary waves, conoid waves and Bessel waves of the (2 + 1)-dimensional Euler equation, Internat. J. Theor. Phys. 46 (2007) 2082–2095.
[45] M. Jia, F. Huang, S.Y. Lou, J.L. Sun, X.Y. Tang, An elastic interaction model of vortices, Commun. Theor. Phys. 54 (2010) 615–618.
[46] J.C. Mcwilliams, An application of equivalent modons to atmospheric blocking, Dyn. Atmos. Oceans 5 (1980) 43–66.

[47] Olga S. Rozanovaa, Jui-Ling Yub, Chin-Kun Hu, Typhoon eye trajectory based on a mathematical model: comparing with observational data, Nonlinear Anal. Real World Appl. 11 (2010) 1847–1861.
[48] http://www.photolib.noaa.gov/htmls/wea00481.htm.
[49] M.A. Lander, G.J. Holland, On the interaction of tropical-cyclone-scale vortices. I: observation, Q. J. R. Meteorol. Soc. 119 (1993) 1347–1361.
[50] http://www.nhc.noaa.gov/2004lisa.shtml.
[51] http://en.wikipedia.org/wiki/Hurricane_Ioke.
[52] http://en.wikipedia.org/wiki/Typhoon_Tip.